Theoretical and Applied Fracture Mechanics 128 (2023) 104086

Contents lists available at ScienceDirect

Theoretical and Applied Fracture Mechanics

journal homepage: www.elsevier.com/locate/tafmec

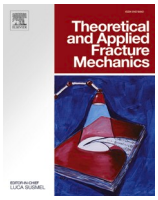

Application of the theory of critical distances for fatigue life assessment of spur gears

G. Cortabitarte [a], I. Llavori [a,*], J.A. Esnaola [a], S. Blasón [b], M. Larrañaga [a], J. Larrañaga [a], A. Arana [a], I. Ulacia [a]

[a] Mechanical and Industrial Manufacturing Department, Mondragon Unibertsitatea, Loramendi 4, 20500 Mondragón, Spain
[b] Dept. of Component Safety, Bundesanstalt für Materialforschung und -prüfung (BAM), Unter den Eichen 87, 12205 Berlin, Germany

ARTICLE INFO

Keywords:
Spur gear
Theory of Critical Distances (TCD)
Multiaxial fatigue

ABSTRACT

This study evaluates the effectiveness of the theory of critical distances (TCD) method in determining the fatigue lifetime of a spur gear. A comprehensive characterization of the material parameters necessary for critical distance calculation was performed, including the fatigue limit and crack growth threshold, as well as σ-N and ε-N curves for 16MnCr5 steel. A variety of TCD methods were applied to analyse the component, including the point method, line method, volume method, and mesh control. The results indicate that overall, the TCD method is a reliable and accurate way to predict the fatigue lifetime of spur gears. The study reveals a strong correlation between predicted and experimental crack locations and fatigue lifetime, suggesting accurate prediction using TCD and the Smith-Watson-Topper parameter. Although all TCD methods, when applied correctly, yield similar results, mesh control is the faster method and is therefore more attractive from an industrial perspective. The results of this study provide valuable insight for engineers and researchers in the field of fatigue analysis of spur gears and similar mechanical components.

1. Introduction

Gears have always been one of the most widely used mechanism in power transmission and there is constant research to try to achieve higher reliability. It is well-known that, due to its working mode, the teeth of a gear are going to be subjected to fluctuating and cyclic loads over time that make fatigue, in most cases, the main cause of failure. These loads generate a stress concentration at the base of the tooth where a crack is generated and propagated over time. In fact, when designing geared transmissions, prevention of such a failure mode is a major goal, and it is supported by standards such as ISO 6336–3 or AGMA 2101.

Lewis was the first to formulate the calculation of stresses at the root of the tooth in 1892 [1]. The gear tooth was considered as a cantilever beam and the most critically stressed position was supposed to be located at the point of tangency of the tooth root with a uniform strength parabola inscribed in the tooth. The calculation method used in AGMA standard is based on this theory. On the other hand, Niemann and Hofer proposed different methods for considering the critical tooth stress. Niemann suggested creating a line from the intersection of the action line of the applied force and the radial centreline of the teeth, specifically, at the tangent point of the tooth profile on the root fillet, and treating that point as a critical stress point [2]. Meanwhile, Hofer considered the tangency point of a 30-degree angle as the critical point in the root fillet [3]. The standards DIN 3990 and ISO 6336–3 are based on this approach. Nowadays, with the computerised definition of the actual gear tooth profile and root geometry, the simplest method for finding the critical section is to directly calculate the stress at a number of points along the fillet, and choose the largest value, also known as Coulbourne method [4].

Nevertheless, from a fatigue point of view, during gear meshing due to load sharing the stress histories at tooth root are different from classical sinusoidal forces with constant amplitude and applied in a fixed direction. Both the force magnitude and direction are variable during gear operation. Therefore, a combination of pure bending and pure compressive stresses could be present. Several approaches have been made to compensate these effects, either experimentally [5] or more recently numerically considering multiaxial fatigue criteria based on the critical plane method [6].

In the multiaxial fatigue literature, special emphasis is placed on the selected criterion being physically representative of the occurring

* Corresponding author.
E-mail address: illavori@mondragon.edu (I. Llavori).

https://doi.org/10.1016/j.tafmec.2023.104086
Received 28 July 2023; Received in revised form 16 August 2023; Accepted 11 September 2023
Available online 19 September 2023

Nomenclature

Symbols

b	the fatigue exponent
c	is the fatigue ductility exponent
E	is the elastic modulus
L	the critical distance
N_f	is the number of cycles to failure
R	load ratio
ΔK_{th}	the fatigue crack propagation threshold
$\Delta\sigma_0$	the fatigue limit range
$\varepsilon_f^{'}$	is the fatigue ductility coefficient
$\varepsilon_{n,a}$	amplitude of the normal strain
σ_0	Point Stress
$\sigma_f^{'}$	is the fatigue strength coefficient
$\sigma_{n,max}$	maximum normal stress

Abbreviations

AM	Area Method
DCPD	Direct Current Potential Drop
DIC	Digital Image Correlation
FCGR	Fatigue Crack Growth Rate
FEM	Finite Element Method
FIP	Fatigue Indicator Parameter
FZG	Forschungsstelle für Zahnräder und Getreibebau (Research Centre for Gears in German)
LM	Line Method
MC	Mesh Control
PF	Plain Fatigue test
PM	Point Method
STBF	Single Tooth Bending Fatigue test
SWT	Smith-Watson-Topper
TCD	Theory of Critical Distances
VM	Volume Method

phenomenon [7]. Therefore, the models are mainly divided into mode I and mode II models. Additionally, there is a multitude of options for analysing the multiaxial criteria. On one hand, a local study can be performed where only the maximum value of each parameter is analysed. On the other hand, non-local methods such as the TCD can be used to take into account the effect of the stress gradient. In recent years, special emphasis has been placed on studying by non-local methods since otherwise very conservative results would be obtained. Within the critical distance theory there are different variants for its implementation, as described in Taylor's book [8].

Regarding the TCD method, a crucial step is obtaining the material data needed to calculate the critical distance. [8]. A common observation in TCD literature, specifically in numerical (finite element method) fatigue studies, is that researchers often opt to utilise literature parameters instead of relying on their own experimental data. This is primarily due to the cost-effectiveness and time-saving benefits associated with this approach, something that Taylor pointed out in his book [8].

In this paper, first, a complete characterization of the material parameters required for the critical distance calculation were performed (fatigue limit and crack growth threshold) as well as σ-*N* and ε-*N* curves. Then, different variants of TCD have been compared with experiments to find out which of the methods is the most suitable in spur gears for the STBF test.

This work is organized into five sections. The first section, the introduction, highlights the need and the novelty of the research being presented. The second section provides the theoretical background concerning TCD. The third section describes both the experimental procedure and the numerical model that were employed in the study. The fourth section presents the results of the research, including the numerical validation of crack location, as well as the assessment of

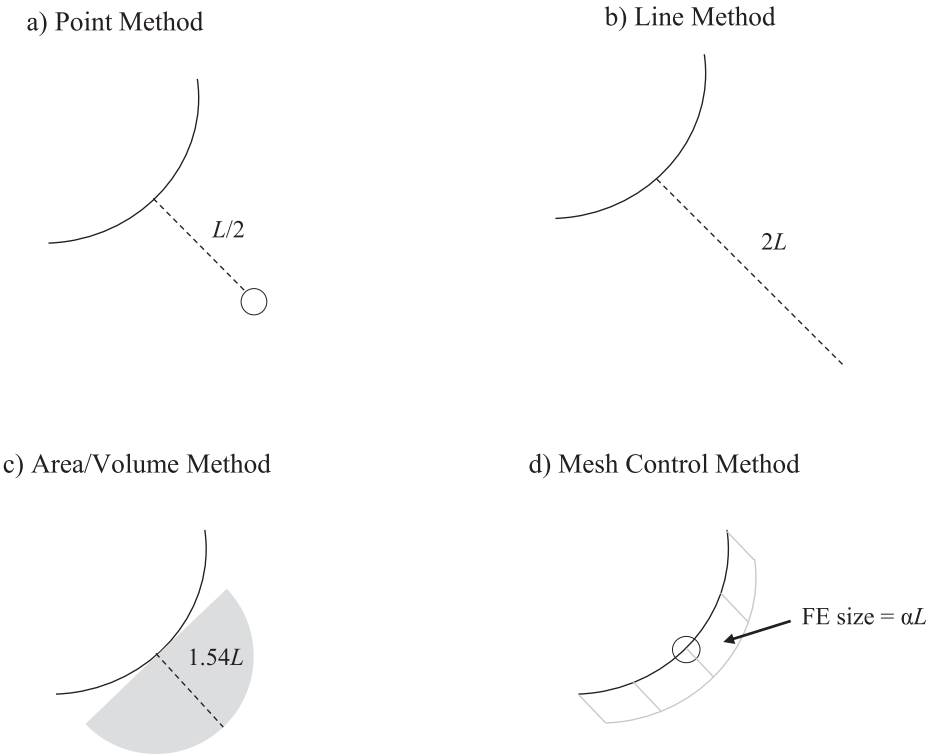

Fig. 1. Schematic of the TCD approaches: a) Point Method (PM), b) Line Method (LM), c) Area/Volume Method (AM/VM), and d) Mesh Control (MC).

fatigue life for different prediction models. Finally, the fifth section summarizes the key findings and conclusions drawn from the study.

2. Background

It is well known that fatigue evaluation at the "hot spot" gives conservative results in notch problems due to the stress gradient effect [9]. To overcome this problem several non-local methods were developed in the literature being the theory of critical distances (TCD) the most widely used approach [8]. The original idea developed by Neuber [10] and then advanced by Taylor decades later can be broken down into several methods, being the Point Method (PM), line method (LM) and volume/area method (VM/AM) the most popular ones. Additionally, during the last years the TCD with Mesh Control (MC) approach arise as a very interesting method due to the computational efficiency as it reduces the simulation time by orders of magnitude [11]. All methods share the idea of a characteristic material length parameter, the critical distance L calculated as

$$L = \frac{1}{\pi}\left(\frac{\Delta K_{th}}{\Delta \sigma_0}\right)^2 \tag{1}$$

where ΔK_{th} is the fatigue crack propagation threshold and $\Delta\sigma_0$ is the fatigue limit range, both related to a particular load ratio.

The PM is the original TCD method and the simplest of all. In this case fatigue failure is predicted when the stresses at a distance of $L/2$, the Point Stress, reaches the fatigue limit (see Fig. 1a),

$$\sigma_0 = \sigma(L/2) \tag{2}$$

In a finite element environment, this method has the problem to obtain a value inside the body in a specific direction, which in complex 3D geometries could be problematic. Additionally, the element size must be refine enough to obtain the value at the specific distance accurately.

The LM uses a focus path to average the stresses over a defined line $2L$ (Fig. 1b)

$$\sigma_0 = \frac{1}{2L}\int_0^{2L} \sigma(r)\mathrm{d}r \tag{3}$$

This method is ideally used for 2D problems, and it is recommended to use structured mesh in order to obtain the stresses at the focus path. Taylor states that the differences between PM and LM are small in the majority of cases, although it is not guaranteed that the estimations will be identical [8].

The AM and VM averages the stress over an area/volume (Fig. 1c). The radius of the circle/sphere is defined as $1.32L$ for the AM and $1.54L$ for the VM [8]. The implementation in the finite element environment is straightforward as it only needs to calculate the Euclidean distance from the focus point to define if the calculated value should be averaged or not. However, in large problems this procedure can be problematic as lots of points are evaluated.

Lastly, the MC theorises that it is possible to use the finite element size multiple of the material length parameter L to average the stresses (Fig. 1d). Therefore, the stress obtained at the hot spot can be used instead of the Point Stress calculated by the PM which eases the calculation process. Furthermore, the MC method has the advantage that large element size can be used, which enables for significant reduction of computational cost and time and could be a cost-effective method for industrial applications. However, the element size might be sensitive to the finite element order and type. Likewise, different finite element code could obtain different results. In this work, an element size of $2.87L$ was selected for the MC approach based on the proportionality of stresses and following the work of Vargiu *et al.* [11].

For a gear tooth failure where a crack originates from the tooth root and is perpendicular to the surface, the Smith-Watson-Topper mode I criterion [12] could be a suitable option. This criterion is defined as the product of the maximum normal stress ($\sigma_{n,max}$) and the amplitude of the normal strain ($\varepsilon_{n,a}$):

$$\mathrm{SWT} = \left(\sigma_{n,max}\varepsilon_{n,a}\right)_{max} = \frac{\sigma_f'^2}{E}\left(2N_f\right)^{2b} + \sigma_f'\varepsilon_f'\left(2N_f\right)^{b+c} \tag{1}$$

where σ_f' is the fatigue strength coefficient, b is the fatigue exponent, E is the elastic modulus, ε_f' is the fatigue ductility coefficient, c is the fatigue ductility exponent, and N_f is the number of cycles to failure. All fatigue parameters are defined for a load ratio of $R = -1$.

3. Methodology

3.1. Material calibration

The material used in this study was 16MnCr5 steel without any heat treatment. The material calibration required for this work was divided into two blocks. The first block focused on characterizing the material's σ-N and ε-N curves to estimate gear fatigue life. The second block involved calibrating the fatigue limit and crack propagation threshold to apply various TCD approaches. Obtaining these experimental results was crucial to ensure the rigorous application of the TCD methodology.

For the characterization of the σ-*N* and ε-*N* curves, the MTS-810 servo-hydraulic machine was used. Cylindrical specimens of 8 mm diameter were manufactured according to the ASTM E466 standard and the two curves were characterized for a stress ratio of $R = -1$. Table 1 and Fig. 2 summarize the test program and the results obtained. In addition, the fatigue limit value was also calculated by means of the σ-*N* curve.

A 100 kN RUMUL resonant machine was used for characterizing the fatigue crack propagation properties of the material. The machine was equipped with an 8-point bending fixture. Single-edge-notched specimens were tested, whose geometry corresponded to $B = 6$ mm, $W = 19$ mm, and $L = 108$ mm. The test setup is shown in Fig. 3. Test frequencies varied along the test according to the stiffness loss while the crack was growing, even though the reference value was approximately 57 Hz. The same load ratio condition tested for the description of σ_a-*N* and ε_a-*N* curves, $R = -1$, was applied.

The direct current potential drop (DCPD) technique [13] was implemented for crack monitoring to achieve the required high resolution for describing propagation rates in the near-threshold regimen. Additionally, the effect of temperature changes in the specimen during the fatigue crack growth rate (FCGR) tests were compensated to avoid

Table 1
Plain fatigue test program results. Results with * symbol were the run-out tests.

Test	σ_a	$\varepsilon_{t,a}$	$\varepsilon_{e,a}$	$\varepsilon_{p,a}$	$2N_f$
–	MPa	–	–	–	Reversals
PF1	–	0.0060	0.002100	0.0039	3,940
PF2	–	0.0060	0.002200	0.0038	3,920
PF3	–	0.0070	0.002150	0.0049	2,648
PF4	–	0.0065	0.002167	0.0043	2,836
PF5	–	0.0050	0.002000	0.0030	5,596
PF6	–	0.0053	0.002033	0.0030	6,202
PF7	–	0.0040	0.001900	0.0021	12,064
PF8	–	0.0070	0.002233	0.0048	1,962
PF9	–	0.0035	0.001900	0.0016	13,462
PF10	–	0.0075	0.002200	0.0053	1,756
PF11	–	0.0025	0.001700	0.0008	51,422
PF12	298	0.001421	0.001421	–	93,800
PF13	259	0.001232	0.001232	–	1,136,000
PF14	219	0.001042	0.001042	–	9,873,692*
PF15	279	0.001326	0.001326	–	285,400
PF16	249	0.001184	0.001184	–	3,184,160
PF17	288	0.001374	0.001374	–	277,840
PF18	269	0.001279	0.001279	–	636,400
PF19	274	0.001303	0.001303	–	938,500
PF20	235	0.001118	0.001118	–	22,307,200*
PF21	239	0.001137	0.001137	–	12,181,970*
PF22	239	0.001137	0.001137	–	20,666,648*

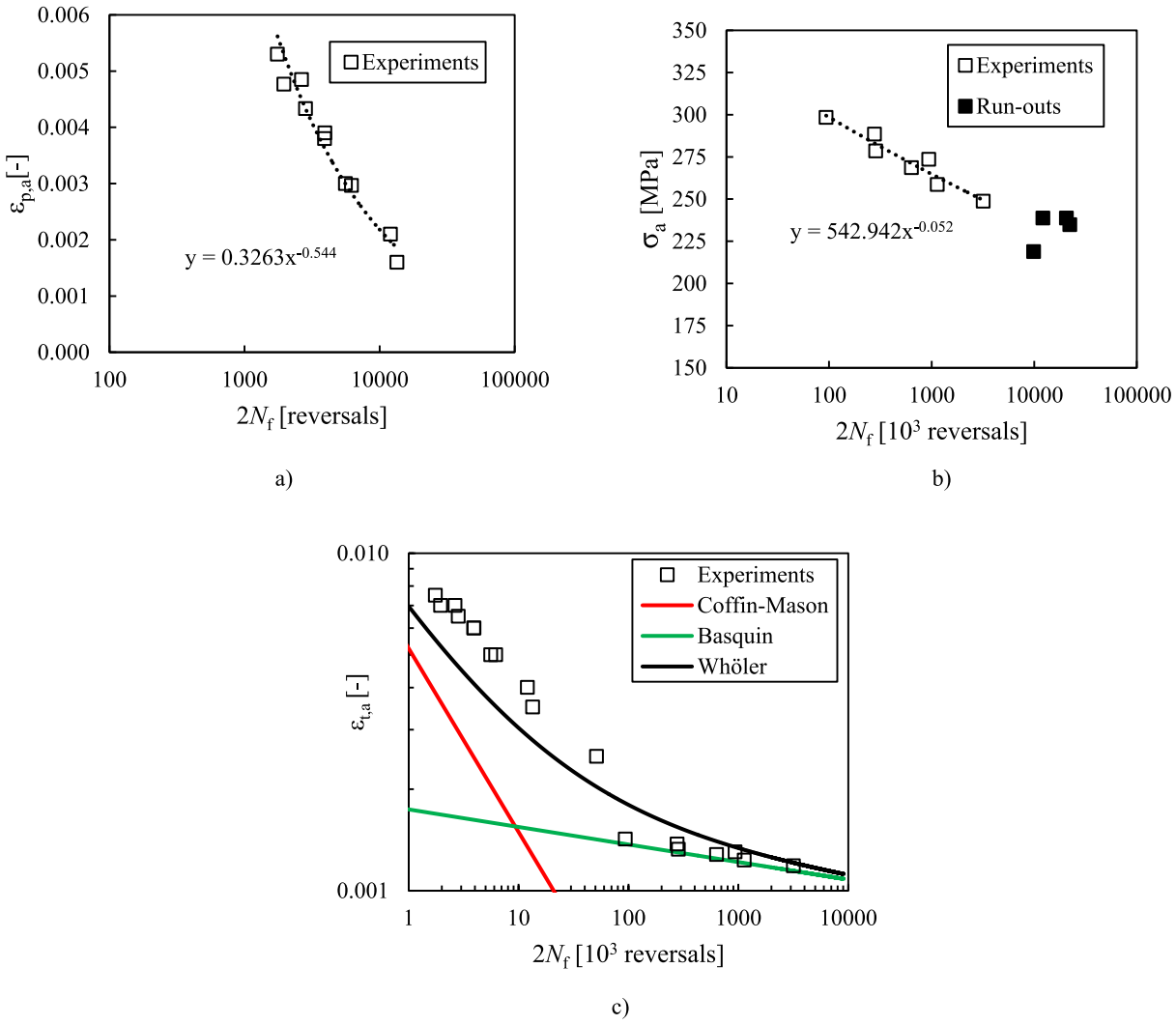

Fig. 2. Experimental data with the calibrated parameters: a) ε-N curve, b) σ-N curve, and c) Whöler curve.

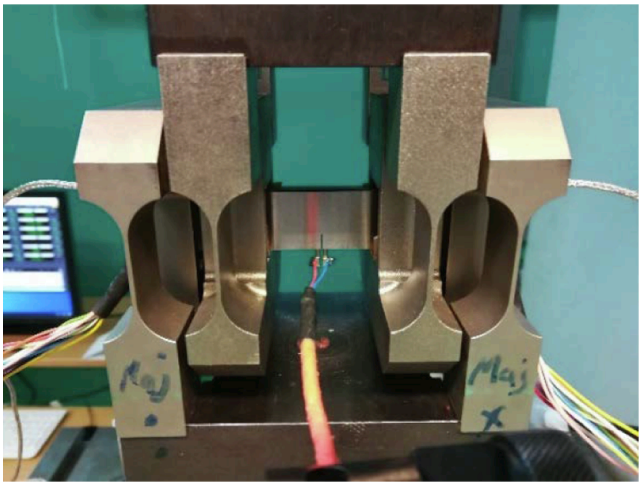

Fig. 3. SEN B8 test setup.

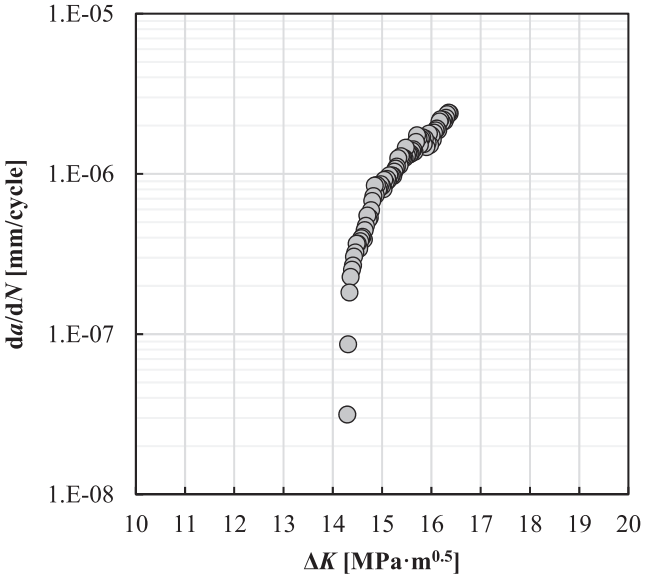

Fig. 4. FCGR results obtained from a 100 kN load capacity resonant machine.

potential and therefore crack-length fluctuations. Furthermore, crack length correction was considered by measuring the initial and final a-values under a microscope by adapting the original fitting parameter in the equation correlating crack size and potential drop ([14]). See [15]

Table 2
Summary of calibrated parameters for fatigue life prediction.

σ_f'	b	ε_f'	c	$\Delta\sigma_{0(10^7)}$	ΔK_{th}	L
MPa	–	–	–	MPa	MPa $m^{1/2}$	μm
542.9	−0.052	0.3263	−0.544	486	13.8	344

for detailed information about the experimental procedure replicated in this research study.

Fig. 4 shows the results obtained after the *K*-decreasing procedure-The threshold value was defined according to the standard ASTM 647 protocol [16].

As summary, Table 2 shows the calibrated parameters values for the applied methodology.

3.2. Single tooth bending fatigue test apparatus

Single tooth bending fatigue (STBF) experiments were carried out using a special tool designed to be mounted in a universal hydraulic fatigue test rig. The peculiarity of this tool, in comparison with most of the tools reported in the state of the art (e.g. [17–18]), is that it allows applying force in both directions and performing fatigue tests with negative stress ratio (R). The vast majority of STBF tools are designed to load the tooth only in one direction, generating tensile bending stresses in the tooth root (i.e. $R > 0$). Meanwhile, gears' loading in normal operating conditions also produces compressive stresses due to the force applied on the preceding tooth. Therefore, tooth root bending fatigue life is affected by the stress ratio as reported by McPherson and Rao [19] when comparing results from STBF tests with FZG running tests.

Fig. 5 shows such tool with the gear mounted on the MTS 810 servo-hydraulic machine. It is composed of a loading push rod supported by journal bearings in order to absorb radial loads. The applied force is measured in the upper fixture which is static while the cyclic load is applied by the movable lower fixture. In order to validate the tooling, it was calibrated in three steps:

i) strain gauges were installed in the loading push rod before and after the tooth in order to compensate the effect of the friction force due to the lower journal bearing;
ii) strain gauges were mounted on both sides of the tooth root in order to verify that loading in both directions was symmetrical;
iii) deformation of the gear tooth was measured using digital image correlation (DIC) by Aramis-GOM in order to verify that the contact point was as designed and consequently the location of the deformation (and stress) of the tooth root were as predicted.

3.3. Single tooth bending fatigue test campaign

The geometry details of the analysed gear are summarized in Table 3. This geometry was selected in order to be able to mount in the developed test rig. Therefore, the highest module was 6 mm (the highest module

Table 3
Manufacturing data of the gear geometry.

Manufacturing data	
Number of teeth	18
Facewidth (mm)	10
Normal module (mm)	6
Helix angle (°)	0
Normal pressure angle (°)	20
Profile shift coefficient	0.178
Tip chamfer (mm)	0.5
Shaft diameter (mm)	40
Tolerance field acc. DIN3967	Cd25
Reference profile acc. ISO53:1998	Profile D (1.4/0.39/1.0)
Quality acc. ISO 1328	5
Surface roughness (μm), Ra / Rz	0.4 / 2

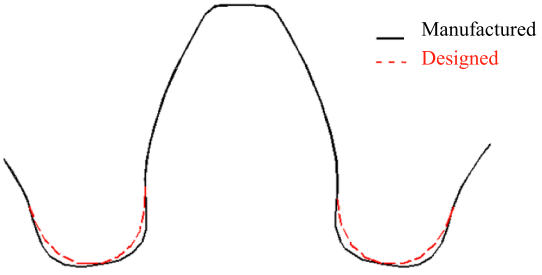

Fig. 6. Tooth root detail showing the differences between designed and manufactured (measured) profile.

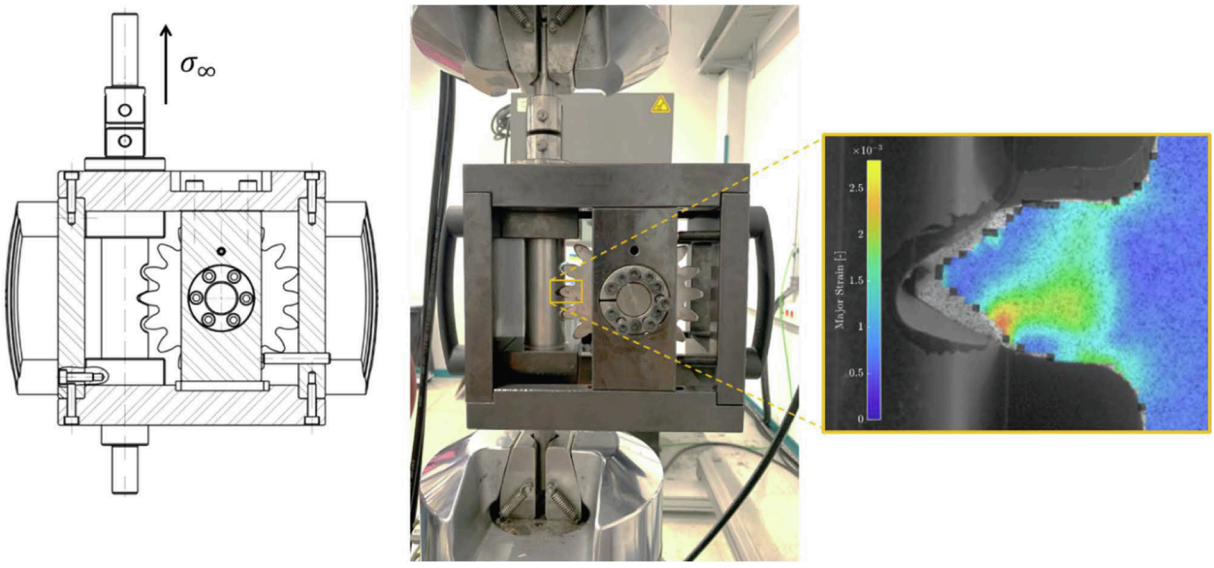

Fig. 5. Detail of the single tooth bending fatigue apparatus. The detail shows the validation of the deformations using digital image correlation (DIC) by Aramis-GOM.

Table 4
Single tooth bending fatigue (STBF) test program results. The asterisk * symbol denotes run-outs tests.

Test	Load	N_f
–	kN	Cycles to failure
STBF1	14	16,849
STBF2	14	16,300
STBF3	12	117,200
STBF4	12	74,500
STBF5	12	50,800
STBF6	11	65,800
STBF7	11	52,300
STBF8	9	72,200
STBF9	9	107,800
STBF10	8	493,400
STBF11	8	912,800
STBF12	7	326,000
STBF13	7	5,045,331*
STBF14	6	6,240,704*

allows us to glue strain gauges in the tooth root) and hobbing tool's deddendum coefficient was chosen to be 1.4 to maximize tooth root stresses. The teeth profiles (including the tooth root) of all the samples were measured before testing using a coordinate measuring machine Mitutoyo Crysta Apex S since the root fillet shape is not usually part of quality control and gear inspection, which are mostly focused on tooth contact area—such as involute form and lead [18]. Fig. 6 compares the manufactured and designed root and it shows that the generated root fillet is not a smooth radius, but a trochoid form due to the grinding wheel. Since root geometry has a direct impact in stress concentration, the numerical analysis considers the manufactured root fillet geometry.

In the present study, the gear was not heat treated as the primary objective of this work is to stablish the correct methodology with the minimum variation on the material properties.

Several loads ranging from 6 −14 kN with $R = 0$ were applied in order to cover the full stress range. Table 4 summarizes the STBF test campaign. Overall, 14 samples (teeth) were satisfactorily tested at 10 Hz frequency.

3.4. Finite element modelling approach

An eight-node brick element (C3D8) was used with further refinement in the root of the gear tooth to define an accurate stress field distribution. Fig. 7 shows the manufactured gear geometry, boundary conditions, applied load and elements used in the numerical model. As shown in the figure, only three teeth were modelled in order to save computational time. As mentioned previously, the selected element size was dependant on the critical distance method. The gear was fixed in the centre using a kinematic coupling to the inner cylindrical surface of the gear. The cyclic force was applied through the push rod and the stresses for the fatigue analysis were recorded at the root of the gear tooth. In this study, the refined mesh on the gear tooth root depicted in Fig. 7 was utilised with point, volume and line methods. On the other hand, the coarser mesh was used with the mesh control method.

4. Results and discussion

4.1. Crack location

The process of validating the numerical procedure used to predict the fatigue life of gear tooth bending involves several steps, one of which is checking the location of the crack in experimental specimens. In order to do this, the maximum tooth root SWT value calculated using the finite element model are compared to the location of the crack in the failed tooth from the test condition.

The crack location of all the teeth was measured using an optical microscope (Leica DMS 1000) as shown in Fig. 8. The average location of the crack initiation is 14 ± 0.23 mm from the tip circumference while the average angle is 27.23° ± 4.51°. This scatter is already reported by other researchers and it could be a consequence of different initial crystal orientations leading to damage taking place on different grains [20].

Fig. 9 shows a general view of the SWT FIP value for the different methods analysed in the study. It is observed that all of them predict the maximum value in a similar location although the values are slightly different. Moreover, it also provides a more in-depth view of the specific location where the maximum SWT fatigue indicator parameter (FIP) occurred in the tooth, as calculated by various methods. The SWT FIP is

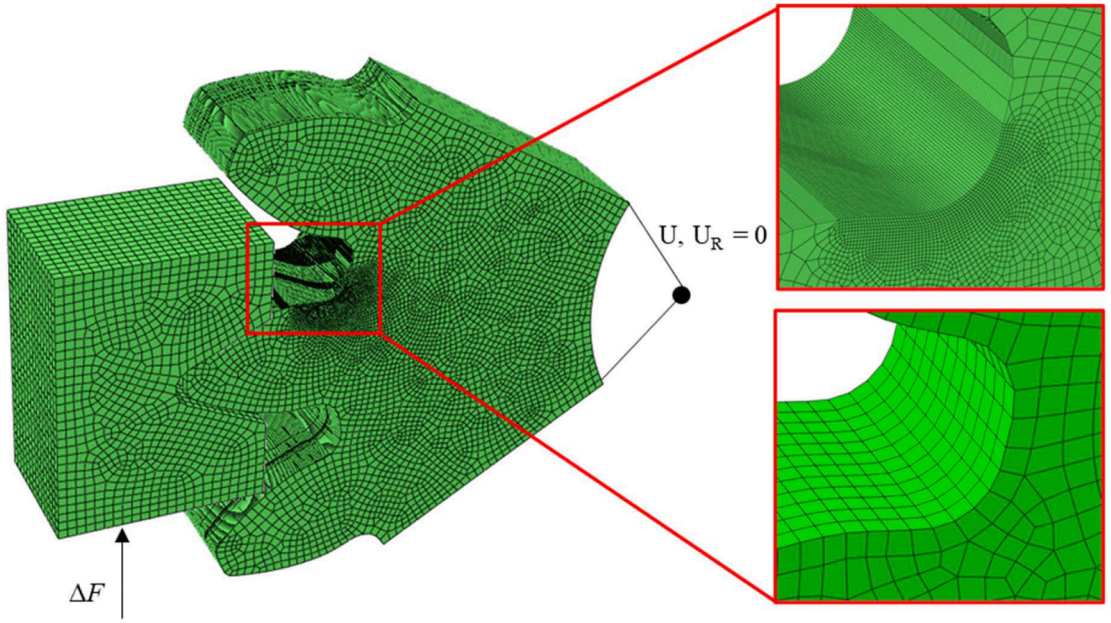

Fig. 7. Finite element model with detail of the fatigue analysis zone highlighting the different element sizes dependent on the selected TCD method. Upper: point method, volume method, and line method; lower: mesh control method.

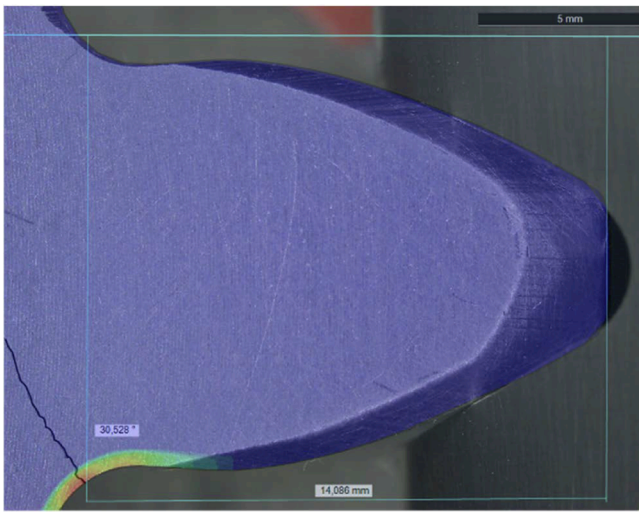

Fig. 8. Measurement of crack location on the tooth root and overlay of the SWT FIP calculated on the failed tooth.

superimposed on an image of the corresponding failed tooth from test condition STBF4/FEM2 (12 kN). This enables comparison of the location of the crack in the experimental sample with the location of the maximum SWT FIP. This information can provide insight into the relationship between the location of the crack and the SWT FIP, which can be useful in understanding the mechanics of tooth failure.

Therefore, it can be concluded that the numerical model fairly represents the mechanical behaviour of the experiment. With this information, the comparison of the fatigue assessment method can be done in the next section with confidence that the numerical model is accurate.

4.2. Experimental correlation and comparison between TCD approaches

In this section, a detailed comparison of the results obtained from the various methods studied in this research is presented. The comparison is divided into two parts: first, the advantages and disadvantages of each of the methods are discussed, and second, the correlation of the results with the experimental tests and the general conclusions are examined.

The overall results of the study are shown in Table 5. In Fig. 10, the results of the maximum SWT value (y axis) obtained with the analysed methods for each of the load cases in Table 5 (x axis) are shown: point method, line method, volume method, and mesh control (different colours in the bar chart). To facilitate the comparison, the differences in absolute percentages with respect to the point method, which was selected as a benchmark as it is the original method developed by Taylor [8], are also shown. From the results, it can be observed that the SWT values from the different methods are quite similar, with the maximum difference being 14% only on one of the tests for the LM approach, and an overall average difference of approximately 3.5%. This suggests that the differences between the methods are relatively small. These results are consistent with the findings of Taylor [8].

Despite the similarities in terms of results obtained from analysed methods, there are significant differences in terms of computational time as shown in Fig. 11. The computational time was calculated by

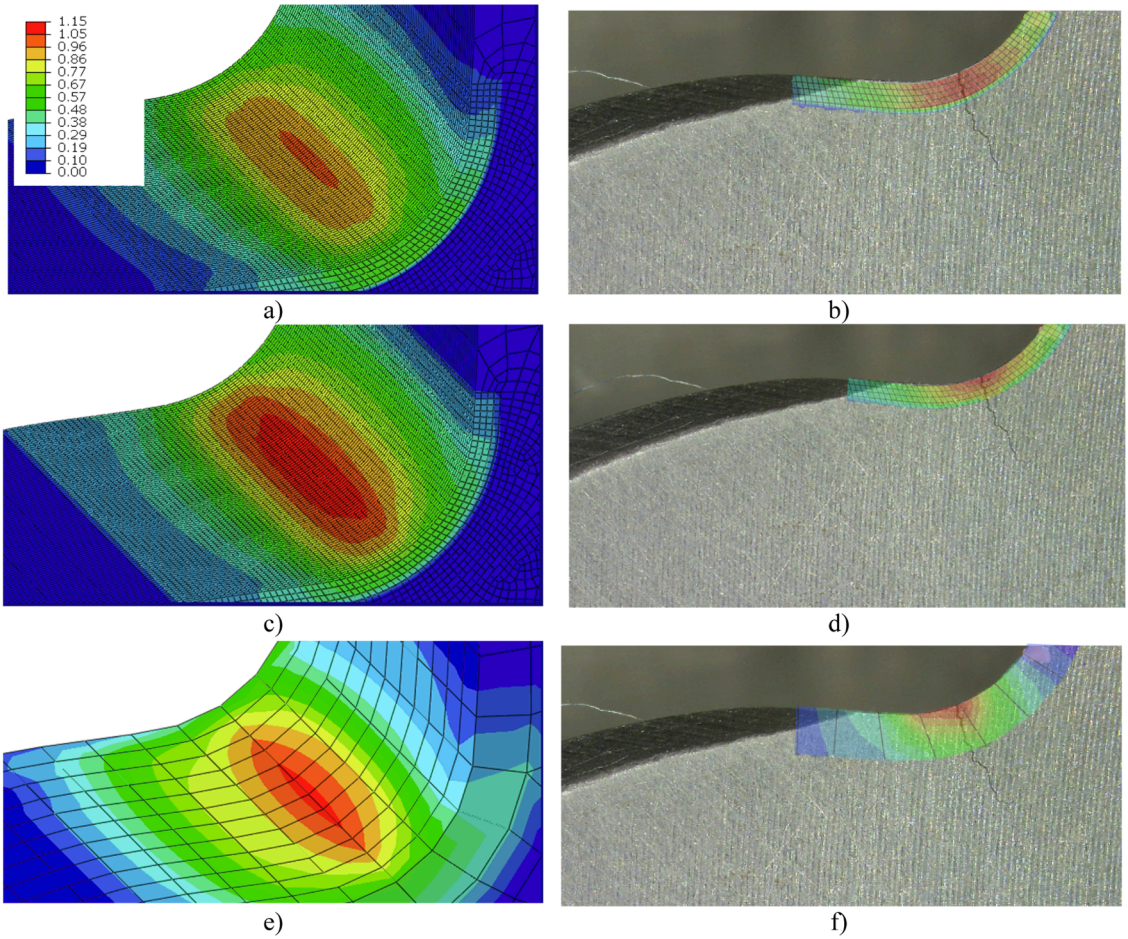

Fig. 9. Comparison of SWT FIP calculated by different methods with a zoomed-in view of the crack initiation point with the finite element mesh: a)-b) volume method, c)-d) point-line method, e)-f) mesh control method.

Table 5
Single tooth bending fatigue FEM results.

Test	Load	SWT PM	N_f PM	SWT VM	N_f VM	SWT LM	N_f LM	SWT MC	N_f MC
–	kN	MPa	–	MPa	–	MPa	–	MPa	–
FEM1	14	0.869	15,179	0.826	17,865	0.841	16,849	0.935	12,113
FEM2	12	0.672	36,583	0.737	26,170	0.766	22,906	0.759	23,668
FEM3	11	0.620	49,902	0.654	40,419	0.628	47,528	0.667	37,621
FEM4	9	0.484	149,529	0.464	185,458	0.485	148,480	0.489	142,152
FEM5	8	0.418	325,805	0.400	422,558	0.416	335,132	0.415	337,189
FEM6	7	0.356	876,632	0.337	1,280,735	0.342	1,158,859	0.337	1,262,551
FEM7	6	0.283	4,708,569	0.263	8,575,210	0.261	9,053,470	0.249	13,773,998

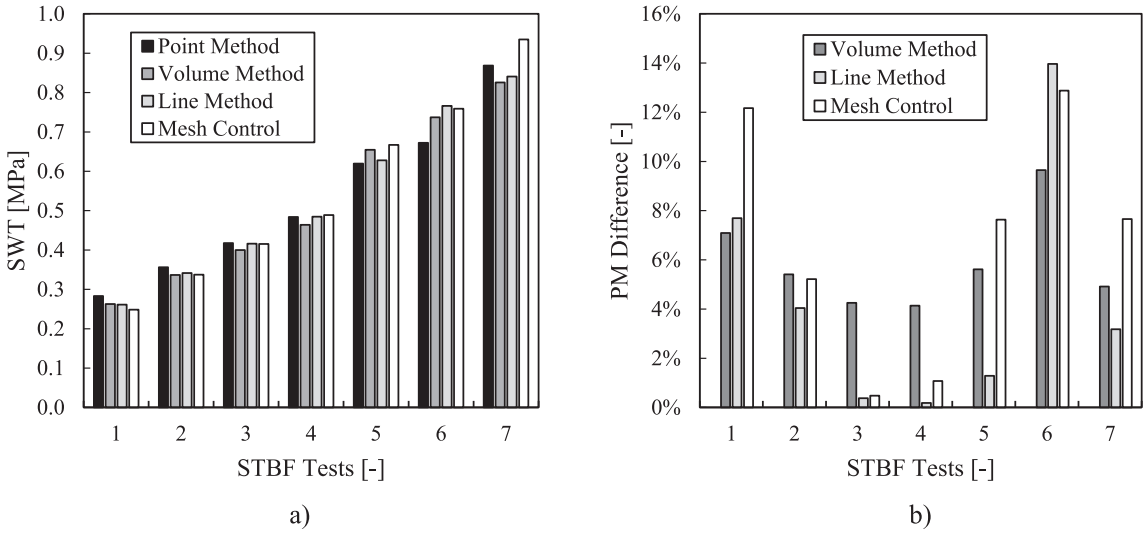

Fig. 10. Comparison of the SWT value for different TCD approaches a), and differences with respect to the Point method b).

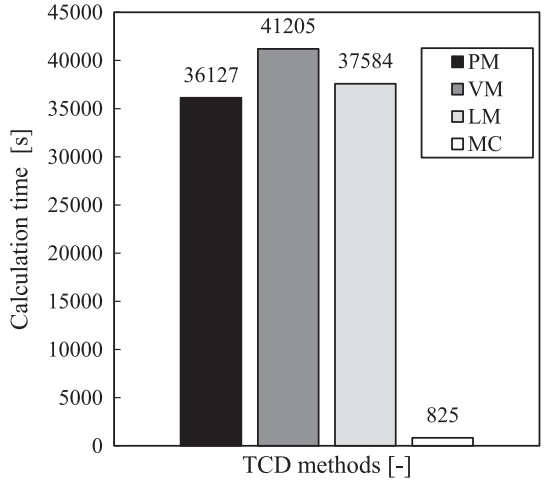

Fig. 11. Comparison of the calculation time (FEM simulation and post-processing) for different TCD approaches.

considering the time required for the finite element method simulation and the post-processing time. The results showed that the volume method is the slowest among the three, with the point method and line method providing similar results. On the other hand, the mesh control method proved to be the fastest, being two orders of magnitude faster than the other methods. This is because the element size required for the mesh control method is considerably larger. It is worth noting that these results might change depending on the specific computer used or the post-processing code employed. Nonetheless, these results clearly demonstrate that the mesh control method is the fastest among the methods analysed in this study.

The experimental correlation for each of the analysed methods is presented in Fig. 12. The results of the study demonstrate that all four methods show a good correlation overall. This means that any of the four methods can be used to obtain accurate results. However, the mesh control method stands out as the most attractive option for this particular study, due to its speed of computation. From the perspective of industry, the mesh control method may also be the most interesting, as it offers a fast and efficient way to obtain good results.

Additionally, the development of artificial intelligence and surrogate modelling has increased the attractiveness of the mesh control method even further. These advanced techniques allow for a large number of simulations to be fed to surrogate models, which can significantly improve the accuracy of results. However, it is important to note that other methods may also be interesting for research purposes. For example, if the effect of a mechanical treatment such as shot peening is being analysed, a refined mesh may be needed to obtain accurate results,

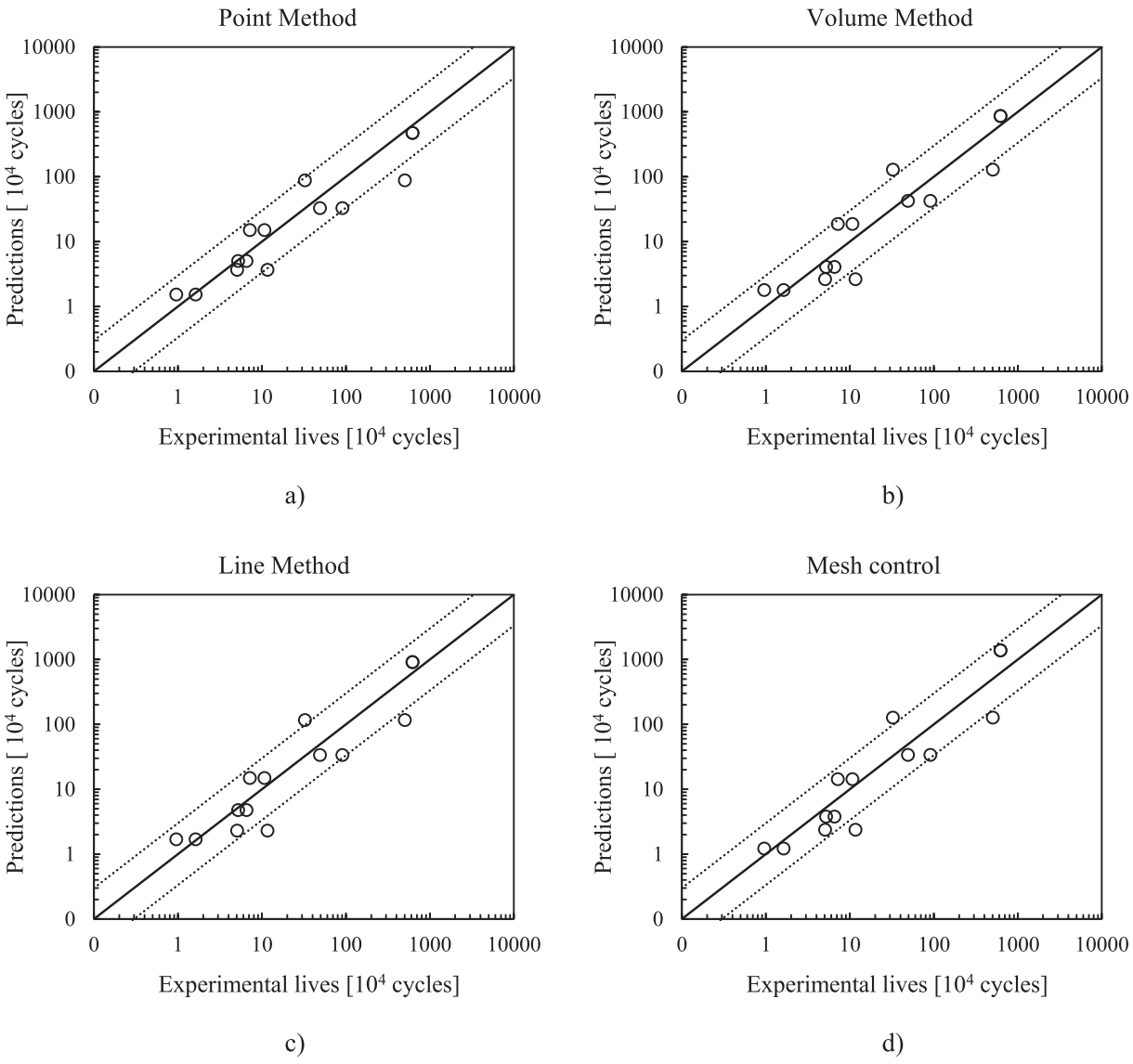

Fig. 12. Correlation between experimental lives and the numerical prediction for different TCD approaches: a) Point Method; b) Volume Method; c) Line Method; and d) Mesh Control.

which may make other methods more suitable. Overall, the results of the study provide valuable insights into the performance of different methods and can guide researchers and practitioners in selecting the most appropriate method for their specific needs.

5. Conclusions

In this study, the effectiveness of the theory of critical distances method in determining the fatigue lifetime of a spur gear was evaluated. Several TCD methods were applied to analyse the component, including point method, line method, volume method and mesh control. A comprehensive characterization of the material parameters necessary for calculating the critical distance was performed, including σ-N and ε-N curves. This approach led to robust results. The results indicate that overall, the TCD method is a reliable and accurate way to predict the fatigue lifetime of spur gears. Based on these results, the following conclusions may be drawn:

- There is a strong correlation between predicted and experimental crack location and fatigue lifetime, with a maximum difference of 14% (only on one of the tests for the LM approach), and an overall average difference of approximately 3.5%. This suggests that the TCD methods combined with the Smith-Watson-Topper fatigue indicator parameter can accurately predict the likelihood of crack formation and failure in spur gears.
- All methods, when applied correctly, yield similar results.
- Mesh control is the faster method and is therefore more attractive from an industrial perspective.
- Other methods may be more suitable for analysing factors such as mechanical treatment or crack growth where a refined mesh might be needed.

Declaration of Generative AI and AI-assisted technologies in the writing process

Statement: During the preparation of this work the authors used GPT4.0 in order to improve readability and language. After using this tool, the authors reviewed and edited the content as needed and take full responsibility for the content of the publication.

CRediT authorship contribution statement

G. Cortabitarte: Conceptualization, Methodology, Validation, Writing – original draft. **I. Llavori:** Conceptualization, Methodology, Validation, Supervision, Resources, Writing – review & editing. **J.A. Esnaola:** Funding acquisition, Methodology, Supervision, Writing – review & editing. **S. Blasón:** Investigation, Data curation, Writing – review & editing. **M. Larrañaga:** Methodology, Supervision, Writing – review & editing. **J. Larrañaga:** Data curation, Supervision, Writing – review & editing. **A. Arana:** Methodology, Formal analysis, Writing – review & editing. **I. Ulacia:** Conceptualization, Methodology, Supervision, Resources, Writing – review & editing.

Declaration of Competing Interest

The authors declare no competing interest.

Data availability

Data will be made available on request.

Acknowledgments

The authors gratefully acknowledge the financial support given by the Diputación Foral de Guipuzcoa under the Project SHOTPENG (Orden Foral 481/2021), the Basque Government under the Project STEINER Grant No. PIBA_2023_1_0052 and the Spanish Government under the Project HYBRID Grant No. PID2021-124245OA-I00 (MINECO/FEDER, UE).

References

[1] W. Lewis, Investigation of the Strength of Gear Teeth, Proc. Engr's Club Philadel 10 (1892) 16–23.
[2] Niemann, G., "Machine Element Design and Calculation in Mechanical Engineering", Vol. II, Gears, Translated by K. Lakshminarayana et al., Springer-Verlag Berlin Heidelberg, New York, 1978.
[3] H. Hofer, Verzahnungskorrekturen an Zahnrädern, Automob. Z. 49 (2) (1947).
[4] J.R. Colbourne. "The Geometry of Involute Gears", Springer-Verlag New York Inc., 1987.
[5] Stahl, K., "Lebensdauer statistik: Abschlussbericht, forschungsvorhaben nr. 304". Technical Report, 580, 1999.
[6] F. Concli, L. Maccioni, L. Bonaiti, Reliable gear design: translation of the results of single tooth bending fatigue tests through the combination of numerical simulations and fatigue criteria, Computational Methods and Experimental Measurements XX (2021) 111–122.
[7] Socie, D., Marquis. G., "Multiaxial Fatigue". SAE, 2000.
[8] D. Taylor, The theory of critical distances: a new perspective in fracture mechanics, Elsevier, 2010.
[9] D. Infante-García, A. Zabala, E. Giner, I. Llavori, On the use of the theory of critical distances with mesh control for fretting fatigue lifetime assessment in complete and nearly complete contact, Theor. Appl. Fract. Mech. 121 (2022), 103476.
[10] H. Neuber, Theory of notch stresses: Principles for exact calculation of strength with reference to structural form and material, Springer Verlag, Berlin, 1958.
[11] A. Zabala, D. Infante-García, E. Giner, S. Goel, J.L. Endrino, I. Llavori, On the use of the theory of critical distances with mesh control for fretting fatigue lifetime assessment, Tribol. Int. 142 (2020), 105985.
[12] K.N. Smith, P. Watson, T.H. Topper, A stress-strain function for the fatigue of metals, J. Mater. 5 (1970) 767–778.
[13] Metals Handbook, Ninth Edition, Vol. 8, Mechanical Testing, J.R. Newby, Coordinator, American Society of Metals, Metals Park. OH., pp. 376–402, 1987.
[14] H.H. Johnson, Calibrating the electric potential method for studying slow crack growth, Mater. Res. Stand. 5 (1965) 442–445.
[15] S. Blasón, T. Werner, J. Kruse, M. Madia, P. Miarka, S. Seitl, M. Benedetti, Determination of fatigue crack growth in the near-threshold regime using small-scale specimens, Theor. Appl. Fract. Mech. 118 (2022), 103224.
[16] ISO 12108. Metallic materials – Fatigue testing – Fatigue crack growth method. International Organization for Standardization (ISO), Geneva, 2018.
[17] A. Singh, An Experimental Investigation of Bending Fatigue Initiation and Propagation Lives, J. Mech. Des. 123 (2001) 431–435.
[18] K. Vučković, I. Galić, Ž. Božić, S. Glodež, Effect of friction in a single-tooth fatigue test, Int. J. Fatigue 114 (2018) 148–158.
[19] D.R. Mcpherson, S.B. Rao, Methodology for translating single tooth bending fatigue data to be comparable to running gear data, Gear Technol. (2008) 42–51.
[20] W. Wang, P. Wei, H. Liu, Y. Yu, H. Zhou, Damage behavior due to rolling contact fatigue and bending fatigue of a gear using crystal plasticity modeling, Fatigue Fract. Eng. Mater. Struct. 44 (10) (2021) 2736–2750.